

# Inferring potential landscapes from noisy trajectories

J. Shepard Bryan IV<sup>\*</sup>,<sup>1</sup> Prithviraj Basak<sup>\*</sup>,<sup>2</sup> John Bechhoefer,<sup>2,\*</sup> and Steve Pressé<sup>1,3,†</sup>

<sup>1</sup>*Department of Physics, Arizona State University, USA*

<sup>2</sup>*Department of Physics, Simon Fraser University, CA*

<sup>3</sup>*School of Molecular Sciences, Arizona State University, USA*

(Dated: February 8, 2022)

While particle trajectories encode information on their governing potentials, potentials can be challenging to robustly extract from trajectories. Measurement errors may corrupt a particle’s position, and sparse sampling of the potential limits data in higher-energy regions such as barriers. We develop a Bayesian method to infer potentials of arbitrary shape alongside measurement noise. As an alternative to Gaussian process priors over potentials, we introduce structured kernel interpolation to the Natural Sciences which allows us to extend our analysis to large data sets. Our method is validated on 1D and 2D experimental trajectories for particles in a feedback trap.

Determining potentials governing particle dynamics is of fundamental relevance to biology [1–5], materials sciences [6, 7], and beyond [8–11]. For example, potentials provide reduced dimensional descriptions of dynamics along a reaction coordinate [2, 4, 5] and yield key estimates of thermodynamic and kinetic quantities [12–14]. Shapes of energy landscapes also provide key insight into molecular function such as the periodic three-well potential of the  $F_0F_1$ -ATP synthase rotary motor [15, 16] and the asymmetric, linearly periodic potentials responsible for kinesin’s processivity [17].

In a different class of applications, fundamental experimental tests of statistical physics [18, 19] often employ potentials with deliberately complex shapes created from feedback traps based on electrical [20, 21], optical [22, 23], or thermal forces [24], or optically generated with phase masks [25] or spatial light modulators [26].

Inferring naturally occurring energy landscapes or verifying artificially created potentials demands a method free of *a priori* assumptions on the potential’s shape. This requirement rules out many commonly used methods devised for harmonic systems [27–30] or alternative, otherwise-limited, methods to deduce potentials from data [8, 31–36]. For example, some methods [31, 32] necessarily rely on binned data, relating potential energies to Boltzmann weights or average apparent force, thereby limiting the frequency of data in each bin and requiring that equilibrium be reached before data acquisition. Other methods assume stitched locally harmonic forms [8]. Still others use neural networks [33] to deduce potentials; the uncertainty originating from measurement error and data sparsity is then not easily propagated to local uncertainty estimates over the inferred potential.

In previous work [37], we introduced a method starting from noiseless one-dimensional time series data to infer effective potential landscapes without binning, or assuming a potential form, or assuming equilibrium conditions, while admitting full posterior inference (and thus error bars or, equivalently, credible intervals) over any candidate potentials arising from sparse data.

Our method was, however, fundamentally limited to

one dimension (because of the poor scaling of the computation with respect to the data set size). It also ignored measurement error and, thus, implications for uncertainty about the potential.

Here we introduce a method to infer potentials from noisy, multidimensional, non-equilibrium data. We take advantage of tools from Bayesian nonparametrics to place priors over arbitrary shaped potentials. To do so, we introduce structured kernel interpolation [38] to the Natural Sciences in order to circumvent the otherwise-prohibitive computational scaling of widely used Gaussian processes. As a result, our method can infer potential shapes from trajectories while meeting all the following criteria simultaneously: 1) no reliance on binning or pre-processing; 2) no assumed analytic potential form; 3) inferences drawn from posteriors, allowing for spatially nonuniform uncertainties to be informed by local density of available data in specific regions of the potential (e.g., fewer data points around barriers); 4) treatment of multidimensional trajectories; 5) rigorous incorporation of measurement noise through likelihoods; and 6) compatible with non-equilibrium trajectories. No other existing method meets all six criteria simultaneously.

*Methods.*—Our goal is to use noisy positional measurements,  $\mathbf{y}_{1:N}$ , to infer all unknowns: 1) the potential at each point in space,  $U(\cdot)$  (with  $U(x)$  denoting the potential evaluated at  $x$ ); 2) the friction coefficient,  $\zeta$ ; 3) the magnitude of the measurement noise,  $\sigma^2$  (under a Gaussian noise model); and 4) the actual position at each time,  $\mathbf{x}_{1:N}$ . Toward achieving our goal, we construct a joint posterior probability distribution over all unknowns. As our posterior does not admit an analytic form, we devise an efficient Monte Carlo strategy to sample from it.

*Data acquisition.*—We performed experiments using a feedback optical tweezer, whose details are given in the SI and have been described in previous work [22]. Briefly, we trap a silica bead of 1.5  $\mu\text{m}$  diameter using an optical tweezer, which creates a harmonic well without feedback. By applying feedback, we change the shape of the potential to a double well along one of the axes. We use two different quadrant photodiodes (QPD) to measure

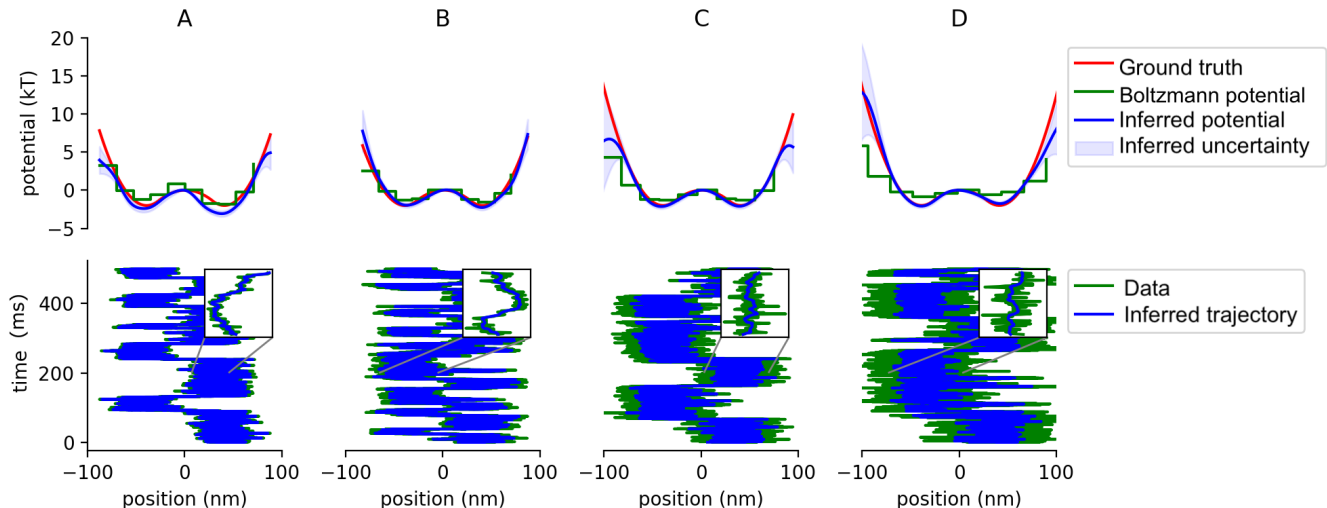


FIG. 1. Demonstration on data from a double-well potential. We analyze four data sets with increasing measurement noise. For each data set, we plot the inferred potential in the top row alongside the ground truth and results of the Boltzmann method. We plot the inferred trajectory against the ground truth in the bottom row. For clarity, we zoom into a region of the trajectory (200 ms to 201 ms). Measurement noise is added by increasing the optical density of the ND filter. The optical densities of the sub-figures A, B, C, D are 0, 0.3, 0.5, 0.7 respectively. Each trace contains 50,000 data points.

the position  $(\mathbf{x}_1, \mathbf{x}_2)$  of a bead at two different values of signal-to-noise ratio (SNR) simultaneously as explained in the supplemental information (SI) [39]. One detector has high SNR and is used for feedback to create the desired virtual potential [40]; the other has an adjustable SNR and is used to explore inferences from measured signals with lower SNR. We reduce the SNR in the other detector by placing neutral density (ND) filters of increasing optical density (OD) in front of it. Thus, we can use our method on the same trajectory over two different experimental SNRs and compare performance. We estimate the measurement noise and SNR in each detector from the noise floor of the power spectrum [39].

*Dynamics.*—We describe the dynamics of the particle with an overdamped Langevin equation [41],

$$\zeta \dot{\mathbf{x}} = \mathbf{f}(\mathbf{x}) + \mathbf{r}(t) \quad (1a)$$

$$\mathbf{f}(\mathbf{x}) = -\nabla U(\mathbf{x}), \quad (1b)$$

where  $\mathbf{x}(t)$  is the possibly multidimensional position coordinate at time  $t$ ;  $\dot{\mathbf{x}}(t)$  is the velocity;  $\mathbf{f}(\mathbf{x})$  is the force at position  $\mathbf{x}(t)$ ; and  $\zeta$  is the friction coefficient. The forces acting on the particle include positional forces  $\mathbf{f}(\mathbf{x})$  expressed as the gradient of a conservative potential,  $\mathbf{f}(\mathbf{x}) = -\nabla U(\mathbf{x})$ . The stochastic (thermal) force,  $\mathbf{r}(t)$ , is defined as follows:

$$\langle \mathbf{r}(t) \rangle = \mathbf{0} \quad (2a)$$

$$\langle r_i(t) r_j(t') \rangle = 2\zeta kT \delta(t - t') \delta_{ij} \quad (2b)$$

where  $\langle \cdot \rangle$  denotes an ensemble average over realizations,  $T$  is the temperature of the bath and  $k$  is Boltzmann's

constant. Under a forward Euler scheme [42] for Eq. (1a) with time points given by  $t_n = n\Delta t$ , each position, given its past realization, is sampled from a normal distribution

$$\mathbf{x}_{n+1} | \mathbf{x}_n, \mathbf{f}(\cdot), \zeta \sim \mathbf{N} \left( \mathbf{x}_n + \frac{\Delta t}{\zeta} \mathbf{f}(\mathbf{x}_n), \gamma^2 \mathbf{I} \right). \quad (3)$$

In words, “the position  $\mathbf{x}_{n+1}$  given quantities  $\mathbf{x}_n, \mathbf{f}(\cdot)$ , and  $\zeta$  is sampled from a Normal distribution with mean  $\mathbf{x}_n + \frac{\Delta t}{\zeta} \mathbf{f}(\mathbf{x}_n)$  and variance  $\gamma^2 = \frac{2\Delta t kT}{\zeta} \mathbf{I}$ .”

As is typical for experimental setups, we use a Gaussian noise model and write

$$\mathbf{y}_n | \mathbf{x}_n, \sigma^2 \sim \mathbf{N}(\mathbf{x}_n, \sigma^2 \mathbf{I}). \quad (4)$$

In words, the above reads “ $\mathbf{y}_n$  given quantities  $\mathbf{x}_n, \sigma^2$  is drawn from a normal.” Here  $\sigma^2$  is the measurement noise variance. In Eq. (4), the measurement process is instantaneous, i.e., assumed to be faster than the dynamical time scales. Our choice of Gaussian measurement model here can be modified at minimal computational cost (e.g., [43]) if warranted by the data.

*Probabilities.*—Next, from the product of the likelihood ( $\mathcal{P}(\mathbf{y}_{1:N} | U(\cdot), \zeta, \mathbf{x}_{1:N}, \sigma^2)$ ) and the prior ( $\mathcal{P}(U(\cdot), \zeta, \mathbf{x}_{1:N}, \sigma^2)$ ), we obtain the posterior over all unknowns

$$\mathcal{P}(U(\cdot), \zeta, \mathbf{x}_{1:N}, \sigma^2 | \mathbf{y}_{1:N}) \propto \mathcal{P}(\mathbf{y}_{1:N} | U(\cdot), \zeta, \mathbf{x}_{1:N}, \sigma^2) \times \mathcal{P}(U(\cdot), \zeta, \mathbf{x}_{1:N}, \sigma^2). \quad (5)$$

The likelihood is derived from the noise model provided in Eq. (4). By contrast, the prior is informed by

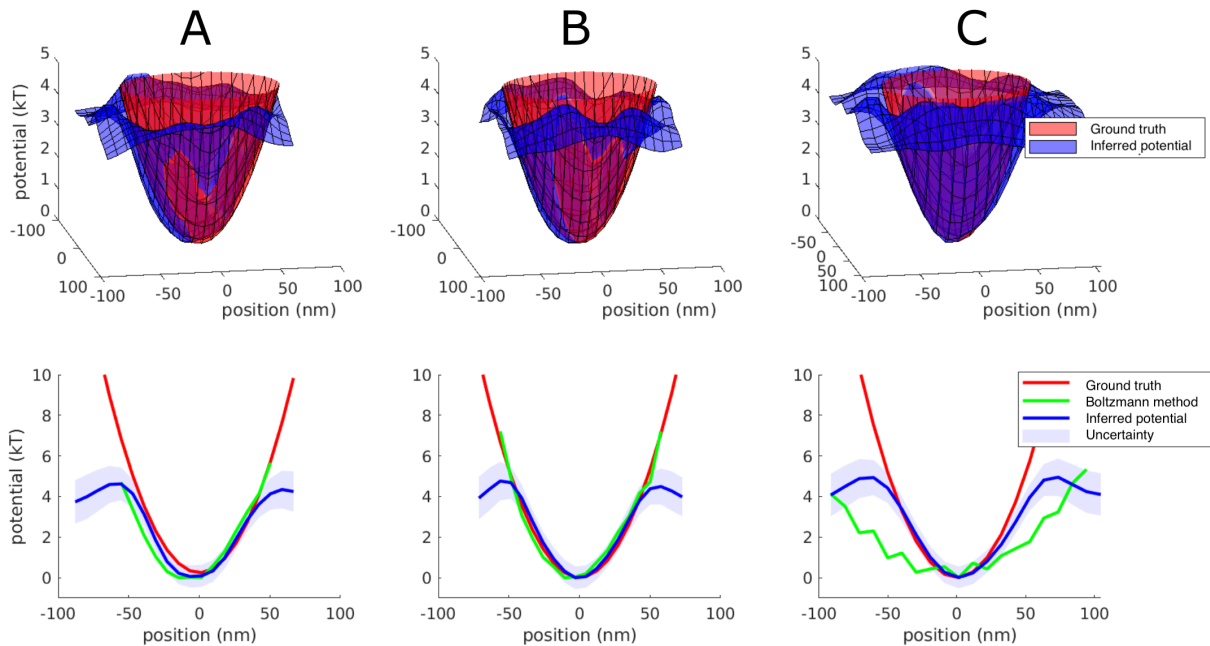


FIG. 2. Demonstration on data from a 2D harmonic potential. Top row: three data sets with increasing measurement noise. Each column shows the inferred potential results along with the ground truth potential for a different data set. At the top we show the inferred potential and ground truth plotted in 2D. Bottom row: 1D slice taken through the middle of the potential. Measurement noise is added by increasing the optical density of the ND filter. The optical densities of ND filter used in the sub-figures A, B, C are 0.0, 0.3, 0.7 respectively.

the Langevin dynamics, as we see by decomposing it as follows:

$$\begin{aligned} \mathcal{P}(U(\cdot), \zeta, \mathbf{x}_{1:N}, \sigma^2) &= \mathcal{P}(\mathbf{x}_{2:N} | \mathbf{x}_1, U(\cdot), \zeta) \\ &\times \mathcal{P}(\mathbf{x}_1 | U(\cdot), \zeta) \mathcal{P}(U(\cdot)) \mathcal{P}(\zeta) \mathcal{P}(\sigma^2). \end{aligned} \quad (6)$$

The first term on the right-hand side of Eq. (6) follows from Eq. (1), while we are free to choose the remaining priors,  $\mathcal{P}(U(\cdot))$ ,  $\mathcal{P}(\mathbf{x}_1 | U(\cdot), \zeta)$ ,  $\mathcal{P}(\zeta)$ , and  $\mathcal{P}(\sigma^2)$ .

Important considerations dictate the prior on the potential. First, the potential may assume any shape (and, as such, is modeled nonparametrically) although it should be smooth (i.e., spatially correlated). A Gaussian process (GP) prior [44] allows us to sample continuous curves with covariance provided by a pre-specified kernel. However, naive GP prior implementations are computationally prohibitive, with time and memory requirements scaling as the number of data points cubed [37, 44].

These size-scaling issues can be resolved by adopting a structured-kernel-interpolation GP (SKI-GP) [38, 45–47] prior for the potential,  $U(\cdot)$ . The SKI-GP prior is a hierarchical structure, where the potential at all points is interpolated according to  $M$  chosen inducing points at fixed locations,  $\mathbf{x}_{1:M}^u$ , and where the values of the potential at the inducing points are themselves drawn from a GP, as detailed in the SI [39]. We note that under this model, we shift the focus from inferring  $U(\cdot)$  to inferring  $\mathbf{u}_{1:M}$  from which we recover  $U(\cdot)$  and  $\mathbf{f}(\cdot)$  with a modi-

fied kernel matrix [39].

Choices for priors on  $\mathbf{x}_1$ ,  $\zeta$  and  $\sigma^2$  are less critical and chosen for computational convenience alone [39].

*Inference.*—As our posterior does not assume an analytical form, we devise an overall Gibbs sampling scheme [48] to draw samples from it. Within this scheme, we start with an initial set of values for the parameters  $(\zeta^{(0)}, \sigma^{(0)}, \mathbf{x}_{1:N}^{(0)}, U(\cdot)^{(0)})$  and then iteratively sample each variable holding all others fixed [49] (see SI [39]).

*Results.*— We benchmark our method on experimental data on a double-well potential and show that we can accurately infer the shape of the potential. We then show that SKI-GP allows us to explore 2D time series data (previously infeasible due to large amounts of data using a naive GP). We finally apply our method to trajectories in a high-barrier landscape where traces are too short to reach equilibrium. A demonstration on data from a simple harmonic well and robustness tests over parameters of interest using simulated data can be found in the SI [39].

For testing the accuracy and effectiveness of GPs method, we simultaneously collected two measurements of each trajectory, one using a detector with low measurement noise and one using a second detector with higher measurement noise. We refer to the low-noise trajectory as the “ground-truth” trajectory, although it itself is subject to a small amount of measurement noise. For each

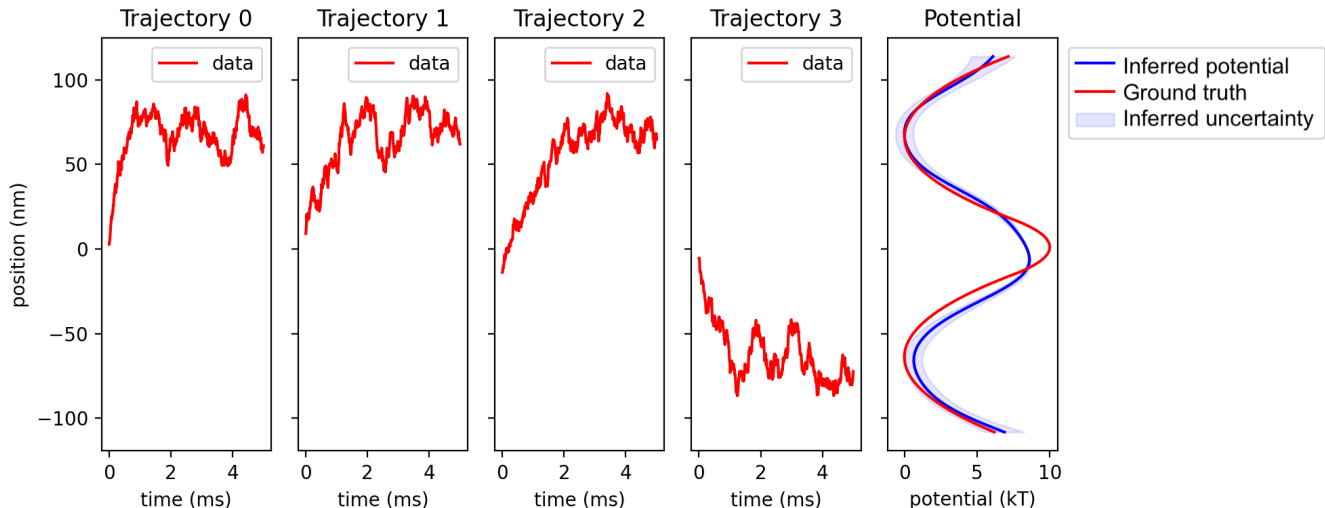


FIG. 3. Demonstration of data from non-equilibrium trajectories. We reconstruct a potential by analyzing many short (500 data points) non-equilibrium trajectories. The left four panels show four of the 100 small data segments used to reconstruct the potential. Each trajectory starts at the top of the potential and rolls off to either side. The far right shows the inferred potential plotted with uncertainty overlaid on the ground truth potential and the potential inferred using the Boltzmann method. For comparison, the inferred and ground truth energy landscapes were shifted so that the lowest point is set to 0  $kT$ .

experiment, we impose a potential on the particle using our feedback trap. We refer to this applied potential as the “ground-truth” potential, although it may differ from the actual potential the particle experiences due to errors in the feedback trap setup, as well as experimental limitations such as drift. We use our ground-truth estimates to validate the accuracy of estimates made using our Gaussian processes on noisy and much shorter time-series data in the SI [39].

*Double well.*—We analyzed data from a particle in a double-well potential. Results are shown in Fig. 1. Each column shows the inferred potential (top row) and inferred trajectory (bottom row) for each data set analyzed. We provide uncertainties and ground truth estimates for both the potential and trajectory. Additionally, for sake of comparison, we also show the potential estimated using the Boltzmann method [31, 37]. We highlight that the Boltzmann method does not provide trajectory estimates. By contrast, our method infers those positions obscured by noise. Fig. 1 shows that the ground truth potential and trajectory fall within the estimated range even when the measurement noise is so large that the particle is occasionally seen in the wrong well (Fig. 1, top right panel). Both our method and the Boltzmann method slightly overestimate the potential of the left well at the lowest noise level, because the (short) trajectory spends too much time in the right well, leaving the left well undersampled.

*2D single well.*—Next, we analyzed data from a particle in a 2D harmonic potential. Results are shown in Fig. 2. For clarity, we do not show uncertainties, trajec-

tories, or Boltzmann-method estimates for the 2D plot, but we do show them for a 1D potential slice. Despite the added complexity in inferring the potential in full 2D at once, our estimates fall within uncertainty in regions where data is appreciably sampled, even at high measurement noise.

*Non-equilibrium trajectories.*—One advantage of our method is that it does not rely on equilibrium assumptions. As such, we can analyze trajectories initiating from non-equilibrium conditions. To demonstrate this, we created data sets where the particle starts at the top of the potential well and “rolls off” to either side. The trajectories are short (5 ms), so that the particle does not reach equilibrium during the time trace. By including the likelihoods from 100 such trajectories into our posterior, we gain information on either side of the well and can recreate the full potential, even though each individual trajectory is initiated from the top of the potential.

In the first four panels of Fig. 3, we illustrate 4 of 100 trajectories used to reconstruct the potential. We note that all trajectories start from the top of the barrier (defined as  $x = 0$ ), and none of the trajectories fully sample both wells. Despite this extreme undersampling, our method is able to infer the height of the barrier to within 15% accuracy (our method predicts an 8.6  $kT$  barrier; the barrier of the design potential is 10  $kT$ ). Our error bar at the top of the barrier in Fig. 3 is artificially low because every trajectory initiates from the top.

*Discussion.*—Inferring potential landscapes is a key step toward providing a reduced dimensional description of complex systems [33, 50–53]. Here, we go beyond exist-

ing methods by providing a means of obtaining potentials, amongst multiple other quantities, from time series data corrupted by measurement noise. We do so by efficiently learning the potential from the rawest form of data, point by point. That is, we achieve this without data pre-processing (e.g., binning), assuming an analytical potential form, nor requiring equilibrium conditions.

As our method is Bayesian, it allows for direct error propagation to the final estimate of the inferred potential shape. In other words, our method differs from others assuming analytic potential forms [54] or projection onto basis functions [34], as well as methods relying on neural nets [53] that cannot currently propagate experimental uncertainty or provide error bars reflecting the amount of data informing the potential at a particular location. Importantly, unlike the Boltzmann method [31], our method does not invoke any equilibrium assumption and can consider trajectories initiated from positions not sampled from an equilibrium distribution. This feature is especially relevant in studying landscapes with rarely sampled regions of space and, in particular, far from non-equilibrium.

As the method is general and the measurement noise model can be tuned, we can apply our method to mapping landscapes from force spectroscopy [55] or even single molecule fluorescence energy transfer [56], with applications to inferring protein conformational dynamics or binding kinetics [57–59]. In inferring smooth potentials, we would move beyond the need to require discrete states inherent to traditional analyses paradigms such as hidden Markov models [60, 61].

---

\* johnb@sfu.ca

† spresse@asu.edu

- [1] D. E. Makarov, *The J. Chem. Phys.* **143**, 194103 (2015).
- [2] J. Wang and A. L. Ferguson, *Phys. Review E* **93**, 032412 (2016).
- [3] J. Wang, S. S. Plotkin, and P. G. Wolynes, *J. de Physique I* **7**, 395 (1997).
- [4] J. Wang and G. M. Verkhivker, *Phys. Review Lett.* **90**, 188101 (2003).
- [5] X. Chu, L. Gan, E. Wang, and J. Wang, *Proc. National Acad. Sci.* **110**, E2342 (2013).
- [6] V. L. Deringer, M. A. Caro, and G. Csányi, *Adv. Mater.* **31**, 1902765 (2019).
- [7] P. H. Handle and F. Sciortino, *The J. Chem. Phys.* **148**, 134505 (2018).
- [8] L. P. García, J. D. Pérez, G. Volpe, A. V. Arzola, and G. Volpe, *Nat. Commun.* **9**, 1 (2018).
- [9] O. K. Dudko, G. Hummer, and A. Szabo, *Phys. Review Lett.* **96**, 108101 (2006).
- [10] H. K. Preisler, A. A. Ager, B. K. Johnson, and J. G. Kie, *Environmetrics* **15**, 643 (2004).
- [11] E. La Nave, S. Mossa, and F. Sciortino, *Phys. Rev. Lett.* **88**, 225701 (2002).
- [12] P. Hänggi, P. Talkner, and M. Borkovec, *Rev. Modern Phys.* **62**, 251 (1990).
- [13] A. M. Berezhkovskii, L. Dagdug, and S. M. Bezrukov, *The J. Phys. Chem. B* **121**, 5455 (2017).
- [14] P. F. Bessarab, V. M. Uzdin, and H. Jónsson, *Zeitschrift für Physikalische Chemie* **227**, 1543 (2013).
- [15] H. Wang and G. Oster, *Nature* **396**, 279 (1998).
- [16] S. Toyabe, H. Ueno, and E. Muneyuki, *EPL (Europhysics Lett.)* **97**, 40004 (2012).
- [17] A. B. Kolomeisky and M. E. Fisher, *Annu. Rev. Phys. Chem.* **58**, 675 (2007).
- [18] K. Proesmans, J. Ehrich, and J. Bechhoefer, *Phys. Review Lett.* **125**, 100602 (2020).
- [19] D. Wu, K. Ghosh, M. Inamdar, H. J. Lee, S. Fraser, K. Dill, and R. Phillips, *Phys. Review Lett.* **103**, 050603 (2009).
- [20] A. E. Cohen, *Phys. Review Lett.* **94**, 118102 (2005).
- [21] M. Gavrilov, Y. Jun, and J. Bechhoefer, in *Optical Trapping and Optical Micromanipulation X*, Vol. 8810 (International Society for Optics and Photonics, 2013) p. 881012.
- [22] A. Kumar and J. Bechhoefer, *Appl. Phys. Lett.* **113**, 183702 (2018).
- [23] J. A. C. Albay, G. Paneru, H. K. Pak, and Y. Jun, *Opt. Express* **26**, 29906 (2018).
- [24] M. Braun, A. P. Bregulla, K. Günther, M. Mertig, and F. Cichos, *Nano Lett.* **15**, 5499 (2015).
- [25] Y. Hayashi, S. Ashihara, T. Shimura, and K. Kuroda, *Opt. Commun.* **281**, 3792 (2008).
- [26] M. Chupeau, J. Gladrow, A. Chepelianskii, U. F. Keyser, and E. Trizac, *Proc. National Acad. Sci. (USA)* **117**, 1383 (2020).
- [27] K. C. Neuman and S. M. Block, *Review Sci. Instruments* **75**, 2787 (2004).
- [28] K. Berg-Sørensen and H. Flyvbjerg, *Review Sci. Instruments* **75**, 594 (2004).
- [29] P. H. Jones, O. M. Maragò, and G. Volpe, *Optical Tweezers: Principles and Applications* (Cambridge University Press, 2015).
- [30] J. Gieseler, J. R. Gomez-Solano, A. Magazzù, I. P. Castillo, L. P. García, M. Gironella-Torrent, X. Viader-Godoy, F. Ritort, G. Pesce, A. V. Arzola, *et al.*, *Adv. Opt. Photonics* **13**, 74 (2021).
- [31] F. Reif, *Fundamentals of Statistical and Thermal Physics* (Waveland Press, 2009).
- [32] S. Türkcan, A. Alexandrou, and J.-B. Masson, *Biophys. Journal* **102**, 2288 (2012).
- [33] J. Wang, S. Olsson, C. Wehmeyer, A. Pérez, N. E. Charron, G. De Fabritiis, F. Noé, and C. Clementi, *ACS Central Sci.* **5**, 755 (2019).
- [34] A. Frishman and P. Ronceray, *Phys. Review X* **10**, 021009 (2020).
- [35] S. Yang, S. W. K. Wong, and S. C. Kou, *Proc. National Acad. Sci.* **118**, e2020397118 (2021).
- [36] A. B. Stilgoe, D. J. Armstrong, and H. Rubinsztein-Dunlop, *Micromachines* **12**, 570 (2021).
- [37] J. S. Bryan IV, I. Sgouralis, and S. Pressé, *The J. Chem. Phys.* **152**, 124106 (2020).
- [38] A. Wilson and H. Nickisch, in *International Conference on Machine Learning* (2015) pp. 1775–1784.
- [39] “Supplemental Material.—the supplementary material contains detailed information regarding the experimental apparatus, data acquisition, and noise calibrations. it also shows the construction of the posterior including

- choices of priors, as well as derivations and computational algorithms used for sampling the posterior using MCMC. it contains a description of the Boltzmann method which we compare our method to. lastly, it has a section devoted to robustness tests on simulated data that we use to benchmark our method.”
- [40] Y. Jun and J. Bechhoefer, *Phys. Review E* **86**, 061106 (2012).
- [41] R. Zwanzig, *Nonequilibrium Statistical Mechanics* (Oxford University Press, 2001).
- [42] R. J. LeVeque, *Finite Difference Methods for Ordinary and Partial Differential Equations: Steady-State and Time-Dependent Problems* (SIAM, 2007).
- [43] M. Hirsch, R. J. Wareham, M. L. Martin-Fernandez, M. P. Hobson, and D. J. Rolfe, *PloS one* **8**, e53671 (2013).
- [44] C. K. I. Williams and C. E. Rasmussen, *Gaussian Processes for Machine Learning*, Vol. 2 (MIT press Cambridge, MA, 2006).
- [45] A. G. Wilson, C. Dann, and H. Nickisch, arXiv preprint arXiv:1511.01870 (2015).
- [46] M. Titsias, in *Artificial Intelligence and Statistics* (PMLR, 2009) pp. 567–574.
- [47] Y. Gal and M. van der Wilk, arXiv preprint arXiv:1402.1412 (2014).
- [48] C. M. Bishop, *Pattern Recognition and Machine Learning* (springer, 2006).
- [49] S. Geman and D. Geman, *IEEE Trans. on Pattern Anal. Mach. Intell.* , 721 (1984).
- [50] S. Chmiela, A. Tkatchenko, H. E. Sauceda, I. Poltavsky, K. T. Schütt, and K.-R. Müller, *Sci. Adv.* **3**, e1603015 (2017).
- [51] P. Espanol and I. Zuniga, *Phys. Chem. Chem. Phys.* **13**, 10538 (2011).
- [52] S. Izvekov and G. A. Voth, *The J. Phys. Chem. B* **109**, 2469 (2005).
- [53] S. Manzhos, R. Dawes, and T. Carrington, *Int. J. Quantum Chem.* **115**, 1012 (2015).
- [54] L. Pérez-García, M. Selin, A. Magazzù, G. Volpe, A. V. Arzola, I. P. Castillo, and G. Volpe, in *Complex Light and Optical Forces XV*, Vol. 11701 (International Society for Optics and Photonics, 2021) p. 1170111.
- [55] A. N. Gupta, A. Vincent, K. Neupane, H. Yu, F. Wang, and M. T. Woodside, *Nat. Commun.* **7**, 631 (2011).
- [56] Z. Kilic, I. Sgouralis, W. Heo, K. Ishii, T. Tahara, and S. Pressé, *Cell Reports Phys. Sci.* **2**, 100409 (2021).
- [57] B. Schuler and W. A. Eaton, *Current Opinion Struct. Biol.* **18**, 16 (2008).
- [58] H. S. Chung and W. A. Eaton, *Current Opinion Struct. Biol.* **48**, 30 (2018).
- [59] F. Sturzenegger, F. Zosel, E. D. Holmstrom, K. J. Buholzer, D. E. Makarov, D. Nettels, and B. Schuler, *Nat. Commun.* **9**, 1 (2018).
- [60] L. Rabiner and B. Juang, *iee assp magazine* **3**, 4 (1986).
- [61] I. Sgouralis and S. Pressé, *Biophys. journal* **112**, 2117 (2017).